Self-organization and dewetting kinetics in sub-10 nm diblock copolymer line/space lithography

Xavier Chevalier, Gwenaelle Pound-Lana, Cindy Gomes Correia, Sébastien Cavalaglio, Benjamin Cabannes-Boué, Frédéric Restagno, Guillaume Miquelard-Garnier, Sébastien Roland, Christophe Navarro, Guillaume Fleury, et al.

Self-organization and dewetting kinetics in sub-10 nm diblock copolymer line/space lithography

Xavier Chevalier,[1] Gwenaelle Pound-Lana,[2] Cindy Gomes Correia,[3] Sébastien Cavalaglio,[2] Benjamin Cabannes-Boué,[3] Frédéric Restagno,[4] Guillaume Miquelard-Garnier,[5] Sébastien Roland,[5] Christophe Navarro,[1] Guillaume Fleury,[3] and Marc Zelsmann[2,*]

[1] ARKEMA France, GRL, Route Nationale 117, BP34, 64170 Lacq, France
[2] Univ. Grenoble Alpes, CNRS, CEA/LETI Minatec, Grenoble INP, LTM, 38000 Grenoble, France
[3] Univ. Bordeaux, CNRS, Bordeaux INP, LCPO, UMR 5629, F-33600, Pessac, France
[4] Laboratoire de Physique des Solides, UMR 8502, Univ. Paris Saclay, 91405 Orsay, France
[5] Laboratoire PIMM, Arts et Metiers Institute of Technology, CNRS, CNAM, HESAM Universite, 75013 Paris, France
[*] Contact author : marc.zelsmann@cea.fr

KEYWORDS: lithography, Directed Self-Assembly (DSA), block copolymers, wetting, thin film stability, nanofabrication

ABSTRACT

In this work, we investigated the self-assembly of a lamellar block copolymer (BCP) under different wetting conditions. We explored the influence of the chemical composition of under-layers and top-coats on the thin film stability, self-assembly kinetics and BCP domain orientation. Three different chemistries were chosen for these surface affinity modifiers and their composition was tuned in order to provide either neutral wetting (i.e. an out-of-plane lamellar structure), or affine wetting conditions (i.e. an in-plane lamellar structure) with respect to a sub-10 nm PS-*b*-PDMSB lamellar system. Using such controlled wetting configurations, the competition between the dewetting of the BCP layer and the self-organization kinetics was explored. We also evaluated the spreading parameter of the BCP films with respect to the configurations of surface-energy modifiers and demonstrated that BCP layers are intrinsically unstable to dewetting in a neutral configuration. Finally, the dewetting mechanisms were evaluated with respect to the different wetting configurations and we clearly observed that the rigidity of the top-coat is a key factor to delay BCP film instability.

INTRODUCTION

Block copolymer (BCP) lithography is considered a very promising alternative lithography technique for sub-10 nm patterning in microelectronics and related applications [1,2]. For resolutions under 10 nm, BCPs with a high Flory-Huggins parameter (so-called high-χ BCPs) have to be designed and are often based on blocks having vastly different surface energies (as compared to the most usual polystyrene-*b*-polymethylmethacrylate (PS-*b*-PMMA) system) [3]. Accordingly, the control of the BCP wetting at the bottom and top interfaces becomes a critical point, as dewetting may occur during the solvent or thermal annealing processes used to promote the BCP self-assembly.

However, the stability of BCP thin films and its competition with the self-assembly mechanisms is barely addressed in the literature, even if numerous studies have been dedicated to the stability of

homopolymer films [4,5]. On a given surface, when the homopolymer film thickness is sufficiently small compared to the capillary length (i.e. the film is not stabilized by gravity), its stability can be described by the spreading parameter S, defined by $S_{hP/X} = \gamma_X - \gamma_{hP} - \gamma_{hP/X}$, with γ_X: surface energy of the surface X, γ_{hP}: surface energy of the homopolymer and $\gamma_{hP/X}$: interfacial tension of the homopolymer on surface X.

For S < 0, the system is thermodynamically unstable and the homopolymer dewets on the substrate, through a spinodal mechanism and/or a nucleation and growth one. Nucleation and growth is usually favored for thicker films, while spinodal dewetting is observed for very thin ones [6]. Conversely, for S ≥ 0, the homopolymer is able to wet the substrate. This latter case only occurs when a strong affinity between the substrate and the homopolymer exists.

The stability of a BCP thin film is more intricate due to the contribution of the phase-separation process. *Brassat et al.* have recently reviewed recent developments on the interplay between BCP self-assembly and dewetting, mainly focusing on the formation of advanced surface architecture [7]. Nevertheless, the complex mechanisms leading to particular dewetted configurations with respect to the self-assembly process or segregation state of the BCP chains are still not fully understood. Indeed, only a few studies have addressed the dewetting of BCP below their order-disorder transition temperature (T_{ODT}), i.e. in a segregated state. Additionally, the role of the self-assembly process on the dewetting dynamics has not been properly answered to the best of our knowledge [8,9]. Above T_{ODT}, i.e. in a molten disordered state, a clearer picture has been drawn, which already depicts some differences compared to the homopolymer case. *Green et al.* [10] studied the dewetting of PS-*b*-PMMA thin films and identified a dewetting dynamics consistent with a slippage regime predicted by *Brochard et al* [6]. Slip between the film and the substrate was attributed to the spontaneous formation of an ordered "brush-like" phase at the film-substrate interface, due to preferential attraction of PMMA towards the substrate (SiO_x in this case). Dewetting occurs because the density of the brush generates an entropic penalty which prevents mixing at the interface. Since the disordered copolymer chains within the film cannot interpenetrate this dense brush, slippage is observed. This mechanism was confirmed by the observation of a 7 nm BCP layer (the size of the "brush") after dewetting on the substrate. This layer, which is a characteristic of autophobic dewetting, has also been identified in other studies [11,12].

Another important difference between BCP and homopolymer films is related to the different affinity of the segregated domains for the top and bottom interfaces. This is well-known in the BCP community, as it will also affect the BCP self-assembly. If the substrate is preferential to a particular BCP block, the corresponding self-assembled domain will wet the substrate leading usually to an in-plane orientation of the BCP structure. This layering will increase the interface potential when the film thickness is incompatible with the optimal layer spacing (intrinsic period). For a BCP film with a free and deformable surface, this effect will result in a quantization of the BCP film thickness as a function of its intrinsic period, i.e. the formation of hole/island features, in order to minimize the free energy of the system.

For line/space applications in lithography, lamellar BCP systems with an out-of-plane orientation of the lamellae (with respect to the substrate) are the targeted structure. To promote this specific organization, "neutral" interfaces have to be designed (i.e. layers presenting a balanced interfacial energy with both BCP blocks). In the case of PS-*b*-PMMA, the interface neutralization is only needed at the bottom interface and is usually performed using a P(S-stat-MMA) copolymer layer (so-called under-layer, UL), having a specific chemical composition. With the advent of high-χ BCP systems, both the top and bottom interfaces have to be modified and neutral top-coats (TCs) were introduced to control the wetting behavior at the top interface. Besides, dewetting becomes even more critical with

high-χ BCP systems as the search of low periodicity requires the design of low molecular weight BCPs more prone to dewetting due to an enhanced chain mobility.
Herein, we choose to compare the impact of different ULs and TCs chemistries associated to a high-χ BCP to investigate the interplay between neutrality, dewetting dynamics, spreading parameters and self-organization kinetics. Here, for the prediction of the thin film stability based on the spreading parameter, we take into account the orientation of the observed self-organized nanomorphologies. The objective of this work is to understand how surface energy modifiers should be designed to prevent dewetting while promoting the desired BCP self-assembly.

EXPERIMENTAL DETAILS

Block copolymer

A lamellar poly(1,1-dimethyl silacyclobutane)-*block*-poly(styrene) (PDMSB-*b*-PS) BCP with a periodicity of 18 nm, called L-DBS18, was used in this study [13,14]. A 0.9 wt% BCP solution in methyl isobutyl ketone (MIBK) was spin-coated at 2000 rpm on various modified Si-substrate (27×27 mm^2 squares cleaved from 200 mm diameter wafers of [1,0,0]-oriented Si) followed by a post-bake step at 60 °C for 1 min, resulting in a BCP layer thickness of 32±2 nm (corresponding to approx. 1.75 periods of the polymer). The T_{ODT} of this polymer was estimated to be around 320 °C (i.e. much higher than used annealing temperatures) from the abrupt drop of the dynamic modulus, G', during isochronal viscoelastic measurements using an Anton Paar MCR 302 rheometer.

Under-layers (ULs)

Under-layers were grafted on the substrate by spin-coating of a 2 wt% solution in MIBK at 700 rpm followed by a thermal grafting at 200 °C for 75 s on a hot plate. Non-grafted material was removed by rinsing with propylene glycol monomethyl ether acetate (PGMEA) under sonication for 10 s, leaving the substrate surface covered with a ~5 nm thick layer (measured by spectroscopic ellipsometry). Three series of grafted under-layers are considered in this study as depicted in Figure 1 and their chemical compositions are detailed in Table 1. Series AA consists of polyalkylacrylate homopolymers (AA), FB are statistical copolymers of 2,2,2-trifluoroethylmethacrylate (F) and butylacrylate (B), and FGH are statistical terpolymers of F, glycidylmethacrylate (G) and 2-hydroxyethylmethacrylate (H). Each type of surface energy modifiers presents a wide range of surface energy in order to define a "neutrality" window for the BCP system under study. Additionally, it allows us to examine the dewetting behavior of the BCP layer for equivalent "neutrality", but for different molecular interactions. For example, the ratios of highly polar and protic F and H co-monomers in the FGH material enables precise tuning of the under-layer surface tension with regards to the BCP (γ_{PDMSB}~27mN.m^{-1}, γ_{PS}~43 mN.m^{-1}), whereby increasing "F" content decreases the surface tension of the FGH material. It is also to be noted that all of these materials are soluble in microelectronic clean-room dedicated solvents, like MIBK, PGMEA or alcoholic solvents.

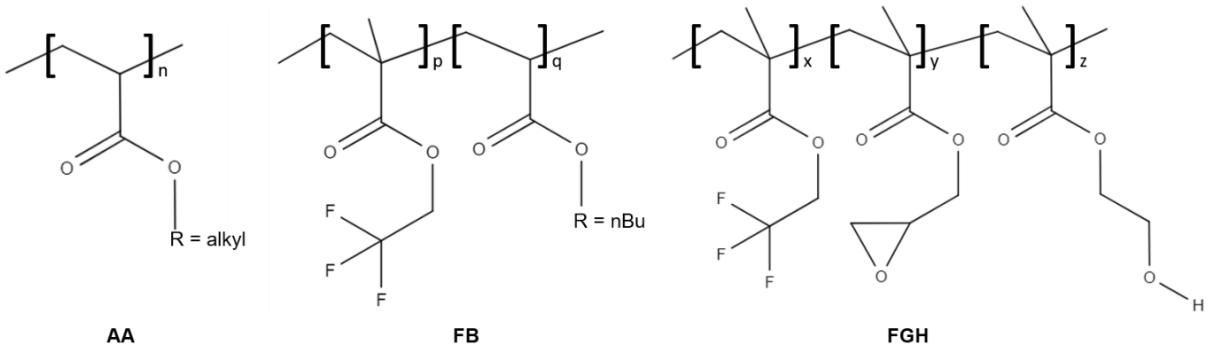

Figure 1. Chemical structure of the under-layer materials designed for the control of BCP wetting. AA under-layers are polyalkylacrylate homopolymers; FB are statistical copolymers of 2,2,2-trifluoroethylmethacrylate (F) and butylacrylate (B); FGH are statistical terpolymers of F, glycidylmethacrylate (G) and 2-hydroxyethylmethacrylate (H).

Table 1. Name, composition and molecular weights of the under-layers used in this study. "gFGH" means grafted FGH material.

Name	Composition	M_n (kg.mol^{-1})
AA-4	poly(butylacrylate)	8.4
AA-6	poly(hexylacrylate)	14.3
AA-8b	poly(2-ethylhexylacrylate)	8.0
AA-8	poly(methylheptylacrylate)	13.8
AA-18	poly(octadecylacrylate)	10.4
FB-50	$F_{50}B_{50}$	11.9
FB-42	$F_{42}B_{58}$	10.4
FB-33	$F_{33}B_{67}$	10.6
FB-17	$F_{17}B_{83}$	10.9
gFGH-76	$F_{76}G_{24}H_{0}$	11.4
gFGH-73	$F_{73}G_{27}H_{0}$	2.8
gFGH-47	$F_{47}G_{27}H_{26}$	2.8
gFGH-37	$F_{37}G_{26}H_{37}$	2.7
gFGH-24	$F_{24}G_{20}H_{56}$	3.0

Top-coats (TCs)

The FGH series can be chemically crosslinked via thermal or UV initiated acid or base catalysis, thanks to the epoxy reactive pendant groups in the G comonomer. Accordingly, this material formulated in solvents orthogonal to the BCP films (1/9 v/v mixture of propylene glycol methyl ether (PGME) and ethanol) was further used as a top-coat. Ammonium triflate or (4-phenylthiophenyl) diphenylsulfonium triflate (10 wt.% vs. FGH) was introduced in the TC solution as ionic thermal catalyst or photo-acid generator, respectively, to enable either thermal or UV-initiated crosslinking of the material. The film was spin-coated on top of the BCP film and annealed at 60°C for 1 min, then cured at 90°C for 3 min (thermally-activated TC) or exposed to UV with a dose of 100 mJ·cm-2 and a post-exposure bake at 90°C for 3 min (photo-activated TC). Slight variations in surface energies are observed between grafted FGH and TCs obtained from the same FGH oligomeric precursor with thermal or UV initiation due to slight differences in chemical compositions of the final material.

Surface energy measurements, interfacial tension and spreading parameter calculations

The contact angles of water, ethylene glycol, and di-iodomethane (ten measurements for each liquid) were measured using a Drop Shape Analyzer (DSA100, KRÜSS GmbH) in a cleanroom environment (23°C, 45% RH). Surface energy polar and dispersive values, γ^P and γ^D, were determined via the Owens, Wendt, Rabel and Kaelble (OWRK) method [15], directly calculated by the *Advance* software provided by *KRÜSS GmbH*. Interfacial tensions of both blocks of the BCP (PS and PDMSB) on these surfaces were

then determined using Wu's equation [16]. The spreading parameter of both BCP blocks on the measured surface X is then given by $S_{Block/X} = \gamma_X - \gamma_{Block} - \gamma_{Block/X}$, with γ_X: surface energy of the surface X, γ_{Block}: surface energy of the block and $\gamma_{Block/X}$: interfacial tension of the block on surface X. For both blocks of the BCP, following values are set from the literature and measurements: $\gamma_{PS} = 43.5$ mN.m^{-1} = $42.1_{DISP} + 1.4_{POL}$ mN.m^{-1}, $\gamma_{PDMSB} = 27.3$ mN.m^{-1} = $25.1_{DISP} + 2.2_{POL}$ mN.m^{-1}. The measured and computed values for all ULs and TCs used in this study are reported in Table 2.

Table 2. Total surface energy (γ^T), dispersive part of the surface energy (γ^D), polar part of the surface energy (γ^P), interfacial tension of PS ($\gamma_{PS/X}$), interfacial tension of PDMSB ($\gamma_{PDMSB/X}$), difference of interfacial tension between PS and PDMSB ($\Delta\gamma i$), spreading parameter of PS ($S_{PS/X}$), spreading parameter of PDMSB ($S_{PDMSB/X}$) and average of the spreading parameters of PS and PDMSB supposing a 1:1 contact area (<S>) for all under-layers and top-coats (X) used in this study. Composition of FGH-23 is $F_{23}G_{19}H_{58}$ and in FGH-0 the fluorinated comonomer F was replaced by tert-butylacrylate ($B_{34}G_{25}H_{42}$). All values are in mN.m^{-1}.

	Name	γ^T	γ^D	γ^P	$\gamma^{PS/X}$	$\gamma_{PDMSB/X}$	$\Delta\gamma_i$	$S_{PS/X}$	$S_{PDMSB/X}$	<S>
UL	AA-18	26.7	26.6	0.1	2.0	0.7	1.3	-21.4	-2.6	-12.0
	AA-8	27.7	26.6	1.1	1.9	0.7	1.2	-19.4	-0.1	-9.7
	AA-8b	29.9	29.2	0.7	2.6	1.1	1.5	-16.2	1.5	-7.3
	AA-6	31.8	30.4	1.4	3.6	0.5	3.1	-13.6	3.8	-4.9
	AA-4	33.6	31.1	2.5	4.6	2.0	2.7	-11.9	5.7	-3.1
	FB-50	23.2	18.9	4.2	10.3	1.6	8.7	-30.6	-5.7	-18.1
	FB-42	24	21	3	7,6	0.5	7,1	-27.1	-3.8	-15.5
	FB-33	26	24	2	5.1	0.03	5	-22.6	-1.3	-11.9
	FB-17	28	27	1	3.4	0.5	2.8	-18.9	0.2	-9.3
	gFGH-76	26.3	23.8	2.5	5.4	0.05	5.3	-21.3	-2.1	-11.7
	gFGH-73	28.2	27.1	1.1	3.3	0.4	2.8	-18.6	0.5	-9.1
	gFGH-47	33.5	30.4	3.1	2.5	0.7	1.9	-12.5	5.5	-3.5
	gFGH-37	35	32.3	2.7	1.7	0.9	0.7	-10.2	6.7	-1.8
	gFGH-24	36.5	31.7	4.8	3.3	1.7	1.6	-10.3	7.5	-1.4
TC	FGH-73	24.6	22.7	1.8	5.9	0.2	5.7	-24.9	-3.0	-13.9
	FGH-47	28.6	25.1	3.5	5.2	0.3	4.9	-20.1	1.0	-9.5
	FGH-37	32.0	27.6	4.4	4.6	0.9	3.8	-16.1	3.8	-6.2
	FGH-24	36.5	30.2	6.3	5.1	2.4	2.6	-12.1	6.7	-2.7
	FGH-23	39.7	34.6	5.1	2.8	2.7	0.2	-6.6	9.7	1.5
	FGH-0	47.7	37.6	10.1	6.8	7.6	0.7	-2.6	12.8	5.1

Thermal and UV annealing

Thermal annealing to promote self-organization of the BCP or crosslinking of TCs was carried out on standard hot-plates in a cleanroom environment (23°C, 45% RH). Unless otherwise stated the annealing time is set to 5 min. UV irradiation was performed with a *Panacol-Eleco UVP280/2*, non-filtered, fibered, mercury arc lamp with a fluence of 1.6 mW.cm^{-2} at a wavelength of 365 nm. Unless otherwise stated the exposure time was 3 min.

Scanning electron microscopy (SEM) and scanning transmission electron microscopy (STEM)

Top-view SEM images were acquired on a *Hitachi CD-SEM H-9300* microscope operating at 0.5 kV electron acceleration voltage with a 6 µA current. Cross-section SEM images were acquired on *a Hitachi S-5000* microscope at 30 kV electron acceleration voltage with a 15 mA emission current. Specimen preparation for STEM imaging was carried out in a *Helios 450S-FEI* dual-beam microscope. First, for samples with a PDMSB layer on top, a thin carbon layer was deposited under electron beam to increase contrast. Then Pt protective layers were deposited on a 30 µm × 2 µm surface area of the sample under electron beam (5 kV, 26 nA, approx. 200 nm of Pt deposited) followed by a 600 nm thick Pt protective layer under focused ion beam (30 kV, 0.43 nA). A 30 µm × 2 µm specimen was then etched away from

the substrate at a depth of approx. 4 µm, transferred to a grid via an Omniprobe needle for mechanical manipulation and thinned under focused ion beam (30 kV, decreasing emission current from 2.5 nA to 80 pA) to approximately 100 nm width. Transmission images of the cross-section were finally recorded in scanning mode at 29 kV and 100 pA on the same equipment using bright field detection.

Dewetting experiments and BCP orientation cartographies

The different multilayered configurations used for the dewetting experiments and for the BCP orientation studies were prepared according to the aforementioned processes. The multilayers were then thermally-annealed to promote the BCP self-assembly. When present, the TC layers were subsequently etched with an ICP plasma based on O_2 or Ar/O_2 chemistries in order to reveal the BCP layer. The samples were then observed with a CD-SEM instrument at a magnification of ×5000 to give 27 µm × 27 µm field-area (or magnification ×10000 with field area of 13.5 µm × 13.5 µm), and around 10 images were randomly recorded for each sample for the dewetting experiments. Pictures were then post-processed using *ImageJ* analysis software from the National Institutes of Health (NIH) (https://imagej.nih.gov/ij/) in order to quantify the proportion of non-dewetted areas.

RESULTS AND DISCUSSIONS

BCP thin film stability below T_{ODT}

Firstly, we investigated the BCP layer stability for all available ULs without any TC. Such conditions are not fully relevant for the configuration of the BCP dewetting process with a crosslinked TC, because of the absence of mechanical confinement and because air is non-neutral to the BCP: the BCP self-organization will produce parallel lamellae at the air interface and change the overall thermodynamic equilibrium conditions. Nevertheless, we believe this experiment is relevant to both compare the BCP chain mobility on these surfaces and understand what drives dewetting for self-assembled polymer thin films.

Optical microscopy images of BCP surfaces after a 3 minute 170°C annealing, i.e. below T_{ODT}, are plotted in Figure 2 for a series of representative ULs. Also, in Table 2, the calculated spreading parameter of both PS and PDMSB blocks are reported for all ULs, as well as the average value for the two blocks (<S>, i.e. the mean spreading parameter that would be relevant in the case of a perpendicular lamellar organization at this interface). In these experiments, in the absence of a neutral layer at the air interface, the wetting of the lower surface energy PDMSB block at the top interface induces a parallel lamellar organization. This is illustrated by STEM cross-section observations for some ULs in Figure 3. It is noteworthy that a symmetric wetting configuration is retrieved for which PDMSB also wets the substrate's interface. Therefore, we have chosen here to describe the observations as a function of the PDMSB spreading parameter $S_{PDMSB/X}$. As shown in Figure 2, we can distinguish three cases depending on $S_{PDMSB/X}$. Not surprisingly, for negative $S_{PDMSB/X}$ values, dewetting occurs in the form of droplets (i.e. the film breaks spontaneously and dewets directly from the substrate in the corresponding timescale). Indeed, droplet formation is the best way to reduce the energy of the system by exposing as much as possible the surface of the low surface energy substrate. For positive values of $S_{PDMSB/X}$, one would expect no dewetting but this is not the case due to the BCP self-assembly inducing the formation of holes and terraces (since the initial film thickness corresponds to about 1.75 periods). For intermediate values of $S_{PDMSB/X}$ ($0 < S_{PDMSB/X} < 5$ mN.m^{-1}), the BCP layer reconfigures with the formation of dewetted holes and islands with maximum height as large as 3 periods (see Figure 3 for AA-8b and gFGH-73 ULs). For higher values of $S_{PDMSB/X}$, the film surface also reconfigures in holes

and terraces, but no dewetting is noticed (i.e. formation of holes of 1 periods and terraces of 2 periods due to the symmetric wetting configuration).

In summary, the segregation of the BCP chains plays an important role on the dewetting and thin film stability below T_{ODT} as the threshold for dewetting appears to be shifted to higher $S_{PDMSB/X}$ values. This, in turn, suggests that the kinetics of self-assembly is faster than the dewetting kinetics, which is a particularly important feature from a technical point of view. It would have been interesting to compare the self-assembly kinetics on different neutral layers, but the process timescale would require the use of in-situ measurements with a fast rate of acquisition (e.g. in-situ grazing incidence small angle X-ray scattering). Besides, while fundamentally interesting, the configuration without TC leads to parallel lamellae that are not the targeted structure for applications in advanced lithography.

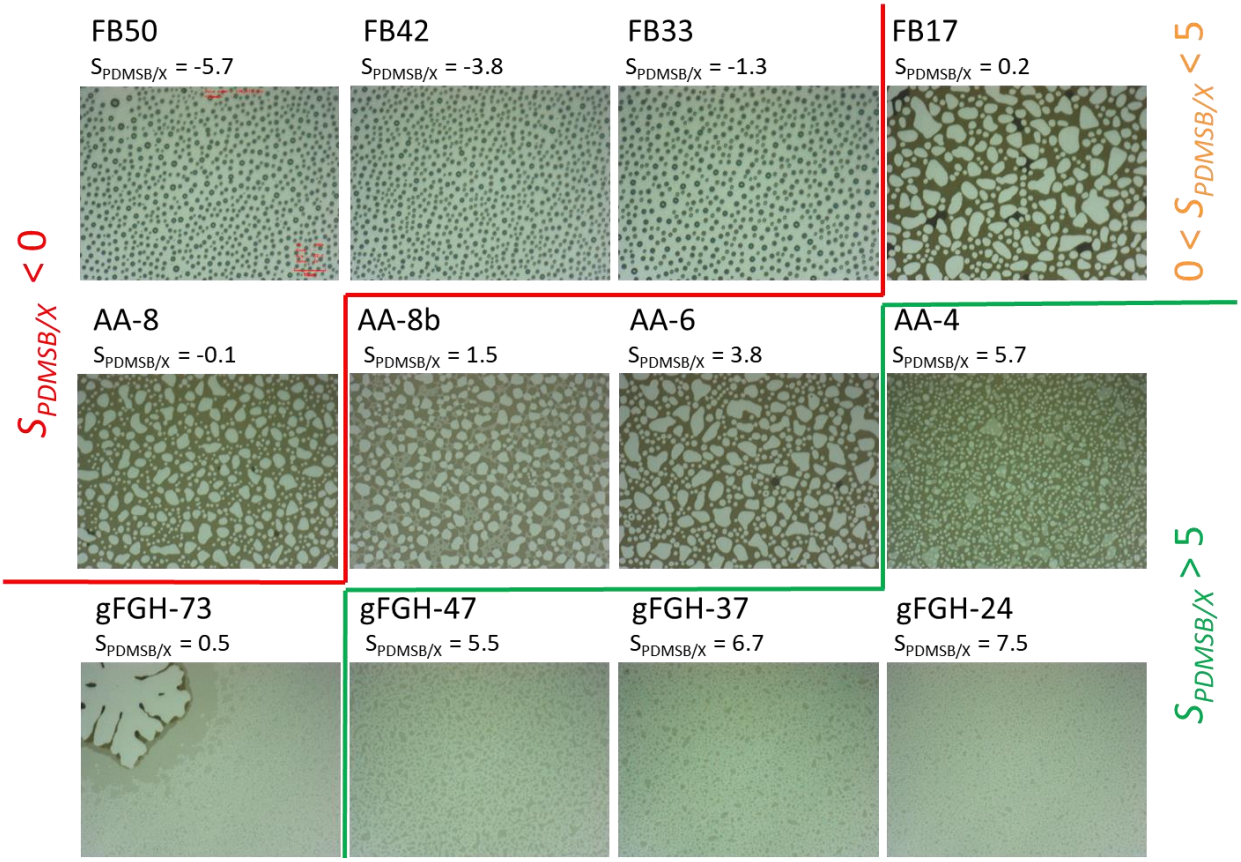

Figure 2. Optical microscope images of the surface of our BCP film after thermal annealing at 170°C for 3 minutes with no top-coat. The calculated spreading factor $S_{PDMSB/X}$ of homo-PDMSB on the surface (in $mN.m^{-1}$) is reported for each surface (assuming a symmetric parallel wetting). Magnification ×100 with field area of 125 µm × 94 µm.

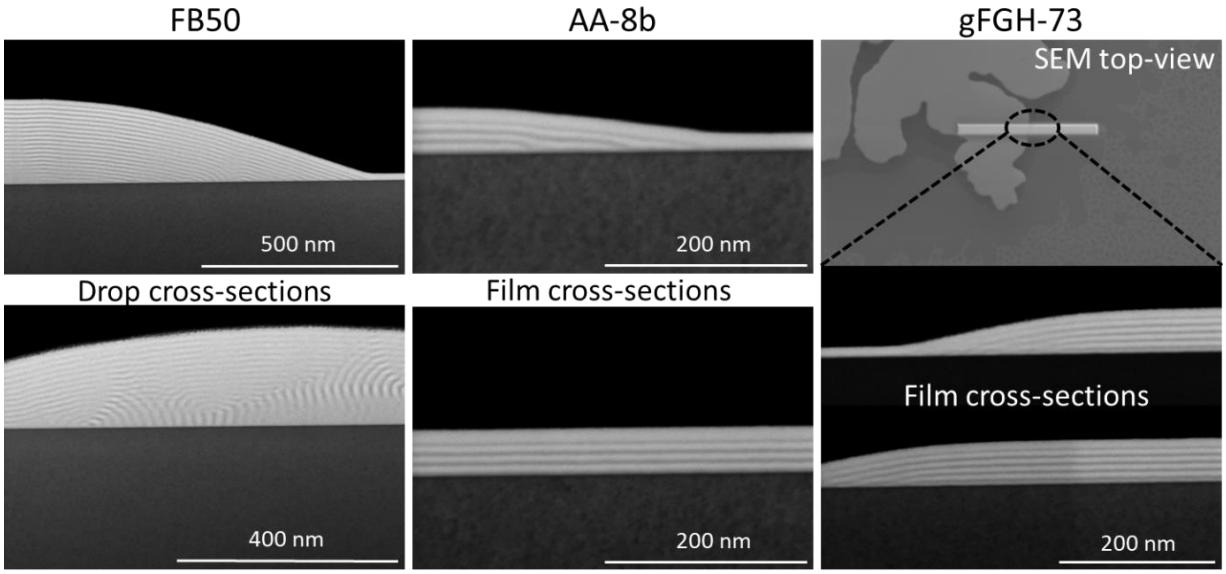

Figure 3. STEM cross-section images of three dewetted samples (three different under-layers) after thermal annealing at 170°C for 3 minutes with no top-coat.

Moreover, dewetting may appear through a spinodal mechanism, probably observed here for lower values of the spreading parameter, or through a nucleation and growth mechanism in a metastable film (see gFGH-73 surface in Figure 2. In this latter case, the large flowers-like features observed on the surface (as opposed to rounded-shape holes) are an evidence of the interrelationship between dewetting and BCP self-assembly below T_{ODT}.

Interestingly, the average spreading parameter <S> (i.e. when considering a perpendicular orientation of the lamellae at the interface) is negative for all considered ULs (Table 2). This means that a perpendicular organization of the lamellar structure is thermodynamically unstable to dewetting for all ULs and in particular for a "neutral" under-layer (NL). In the next section, we aim to clarify some of the aspects of this particular NL/BCP configuration in order to explain this instability.

Neutrality and BCP thin film stability

The NLs considered in this study consist of a polymer brush grafted to the substrate. Technological constraints (e.g., plasma etching of patterns) dictate that this layer should not be too thick (≈ 5 nm). Thus, the grafted chains generally have a lower molecular weight than the BCP chains. Here, we are working with relatively short grafted chains (Mn approx. 10 kg.mol^{-1} or lower, see Table 1), which tends to form densely grafted layers and therefore is favorable to autophobic dewetting [17,18]. In addition, the NL chemical composition must be taken into account. It may be based on the same chemistry as the BCP chains (*e.g.*, the PS-*stat*-PMMA copolymer used to control PS-*b*-PMMA self-assembly), or be based on different repeating units but without specific attractive interactions with them (i.e. without a negative χ parameter). Then, the presence of a constituent with a repulsive interaction (i.e. with a positive χ parameter) for a given block (*e.g.*, the MMA unit of NL versus the S unit of the BCP), generates an additional enthalpic cost for BCP penetration into the neutral brush layer, which further destabilizes the film. Finally, in all cases, without attractive interactions between the NL and the BCP blocks and favorable van der Waals interactions, the dewetting of the BCP on a neutral layer occurs due to both entropic and enthalpic penalties.

The global spreading parameter for a BCP layer on a neutral layer can be written as $S_{BCP} = \gamma_{NL} - \gamma_{BCP} - \gamma_{BCP/NL}$, with γ_{NL}: surface energy of the neutral surface, γ_{BCP}: surface energy of the BCP and $\gamma_{BCP/NL}$:

interfacial tension of the BCP on the NL. For a symmetric A-*b*-B BCP with a perpendicular orientation of its domains, the surface energy of the BCP can be rewritten as $\gamma_{BCP} = ½ (\gamma_A + \gamma_B)$. Assuming the same overall composition between the symmetric BCP and the NL made of the same constituents, we have also $\gamma_{NL} = ½ (\gamma_A + \gamma_B)$. Besides, the neutrality condition at the NL/BCP interface leads to $\gamma_{BCP/NL} = \gamma_{A/NL} = \gamma_{B/NL}$. Accordingly, the expression of S_{BCP} can be simplified to $S_{BCP} = -\gamma_{A/NL}$. Therefore, in this particular case, the spreading parameter is negative and the BCP is indeed thermodynamically unstable on a NL containing similar repeating units (assuming that long-range contributions are ignored). The pioneering study by *Mansky et al.* on surface neutralization for the PS-*b*-PMMA system provides striking evidence for this behavior [19]. In this work, PS and PMMA homopolymers are metastable on their chemically similar brushes. However, this metastable state becomes truly unstable when these homopolymers are deposited on PS-*stat*-PMMA layers and in particular those with a neutral composition for the BCP. The demonstration of the dewetting of PS-*b*-PMMA thin films on their NLs was subsequently established [20,21].

In the case of a NL composed of chemically distinct repeating units with respect to the BCP, additional parameters must be considered. Indeed, the enthalpic contribution of repulsive or attractive interactions between each of the NL constituents and each of the BCP segments will have an effect on $\gamma_{BCP/NL}$. On the one hand, repulsive interactions destabilize the film by adding a positive enthalpic contribution to $\gamma_{BCP/NL}$. On the other hand, attractive interactions could stabilize the BCP layer by promoting mixing at the NL/BCP interface. However, even if such attractive interactions are present between the NL and BCP domains (with the same magnitude for each block to maintain neutrality), autophobic dewetting of the BCP chains above a strongly anchored BCP layer could still occur, as observed by *Epps et al.* in the case of a tri-block copolymer system [22].

In conclusion, rather than pursuing the thermodynamic stability of the BCP layer, we can more simply require that it is kinetically stable. In the ultra-clean semiconductor environment, there are very few impurities to nucleate holes in a metastable BCP film. Therefore, we can consider only the stability of the BCP film with respect to spinodal dewetting, i.e., the spontaneous growth of film thickness variations. The spinodal dewetting is governed by the curvature of the interface potential, which in turn is mainly determined by the thickness-dependent long-range van der Waals interactions between interfaces. Due to the very thin thickness of the films generally used in BCP lithography (15-35 nm), we find ourselves in a regime where these interactions can play a role and a judicious choice of materials may kinetically stabilize the BCP film. Indeed, this may explain the differences observed previously on the dewetting patterns of two different surfaces in Figure 2: gFGH-73 and AA-8b surfaces. In both cases the lamellae orientation is parallel to the substrate (as evidenced Figure 3) and the spreading parameters are similar (the one that has to be considered here is $S_{PDMSB/X}$ in Table 2 due to this parallel wetting). As said before, the large flower-shaped features observed on the gFGH-73 surface characterize nucleation of dewetting on impurities in the case of a metastable film, while the finer patterns in the case of the AA-8b surface is consistent with a spinodal dewetting. Another clue that the dewetting mechanism on these two surfaces involves different mechanisms is related to the behavior observed with the addition of a cross-linked top-coat. As evidenced in Figure 4, the dewetting can be cancelled by the top-coat in the case of gFGH-73 treated surfaces, whereas dewetting still occurs on the AA-8b surface under comparable conditions (and yet with the needed neutral wetting conditions at both interfaces in both cases). In summary, neutral layers with different chemistries may present different dewetting dynamics.

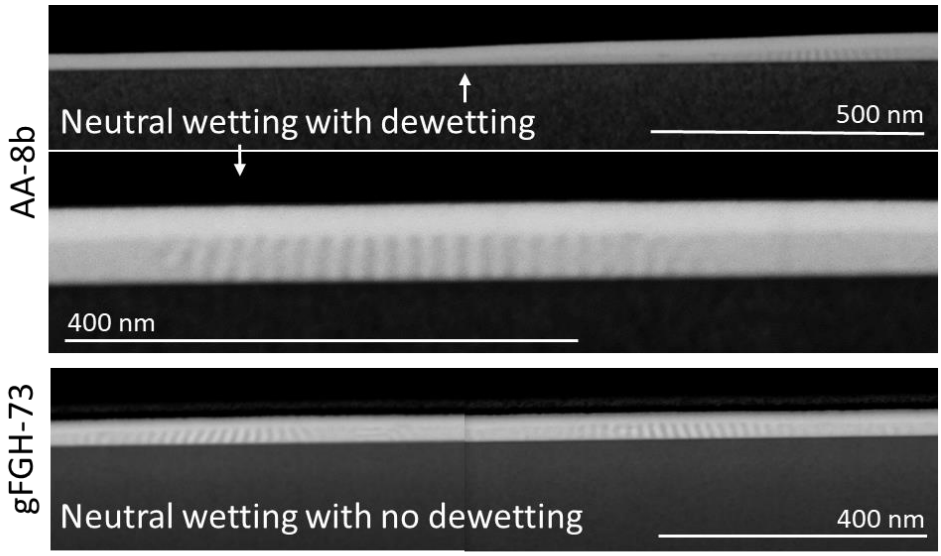

Figure 4. STEM cross-section images of two samples with different surface treatments and same crosslinked top-coat after thermal annealing at 240°C for 5 minutes. Cross-linking of the FGH-47 TCs by UV (180 mJ.cm^{-2}) followed by a 90°C-3 minutes bake.

Dewetting kinetics in neutral conditions with a crosslinked TC

As evidenced in Figure 4, a rigid crosslinked TC can delay or suppress dewetting [14]. A more detailed study on the influence of the degree of TC crosslinking on the dewetting kinetics was undertaken with a AA-8 UL and a UV-crosslinkable FGH-37 TC. Under these conditions, the wetting at both interfaces is neutral (see Figure 6 in next section). Three different UV doses were used to modulate the degree of crosslinking and the ratio of dewetted area after thermal annealing at 140°C for different bake time is presented in Figure 5. This study shows a delayed dewetting under all three TC stiffness conditions leading to a sharp reduction of the dry area with the increase of the TC stiffness. Thus, this approach appears as an elegant technical solution to control the occurrence of dewetting under practical nanofabrication conditions. It is further probed in the next section to investigate various UL/TC combinations associated to the high-χ BCP layer.

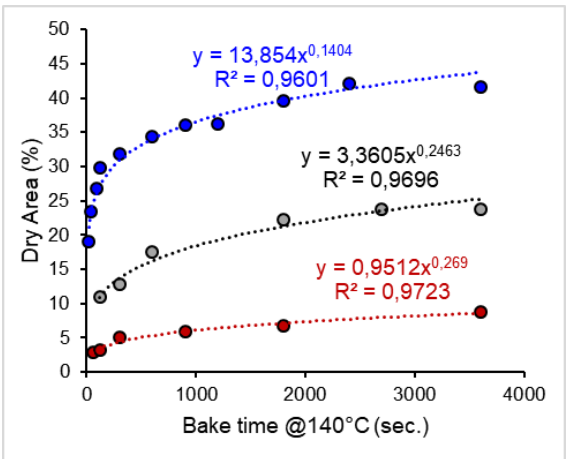

Figure 5. Dewetting kinetics of a symmetric BCP layer with a partially UV crosslinked FGH37 TC and a AA-8 neutral UL (UV dose: blue: 45 mJ.cm^{-2}, grey: 90 mJ.cm^{-2}, red: 180 mJ.cm^{-2}). The area of dry holes in the BCP layer is monitored as function of self-assembly bake time. The dotted lines are the ones for the power-law best-fit of each data set. 7 randomly taken SEM images are used for each sample (one sample per time increment).

Influence of UL and TC on BCP lamellae orientation and film stability

Finally, we investigated the BCP lamellae orientation and film stability for all available combinations between ULs and TCs. Typical SEM images of the BCP surface after TC etching are presented in Figure 6,Figure 7 andFigure 8 and are classified according to the surface energies measured for the UL and TC (so-called cartographies). Neutral conditions leading to perpendicular lamellas are highlighted with a green frame. The same TC series is used in the three experiments while Figure 6 presents the results for the AA series used as ULs (annealing temperature 240 °C for 5 min), Figure 7 presents the results for the FB series used as ULs (170°C / 5 min) and Figure 8 presents the results for the grafted FGH series used as ULs (260°C / 5 min).

Drastic differences in film stability are observed between the UL series. An extended dewetting is observed in the case of the FB series whereas dewetting is only observed for extreme values of surface energies in the two other cartographies. Indeed, non-neutral wetting conditions at interfaces favor dewetting as the resulting parallel lamellar configurations can no longer minimize their free energy by forming holes and islands due to the presence of the rigid top-coat. From a thermodynamic point of view, this therefore destabilizes the parallel lamellar configuration and favors perpendicular lamellae (which is preferable from a nanofabrication point of view) [23,24]. The fact that no dewetting is observed for the AA and gFGH series for the central values of the surface energies appears at first sight contradictory with the results obtained previously. It is linked to a competition between the cross-linking process and the dewetting kinetics on these particular ULs. We hypothesize that the completion of the TC cross-linking proceeds during the thermal annealing step at elevated temperature and yields a stiff layer inhibiting dewetting phenomena for the AA and gFGH series. This competition between stiffening of the TC and dewetting is nevertheless not sufficient to inhibit dewetting for the FB series due to highly unfavorable <S> values (i.e. accelerating the dewetting kinetics).

The stability of the sandwiched BCP layers can be related to the calculated average spreading parameter of the two BCP blocks (<S> in Table 2, when considering a perpendicular organization). A first observation is that extended dewetting, as observed for the FB series, generally correlates with a strongly negative <S> value. It should be noted, however, that the magnitude of <S> is only indicative because it only takes into account the interface with the substrate (or the TC) and does not take into account the mechanical confinement by the rigid TC.

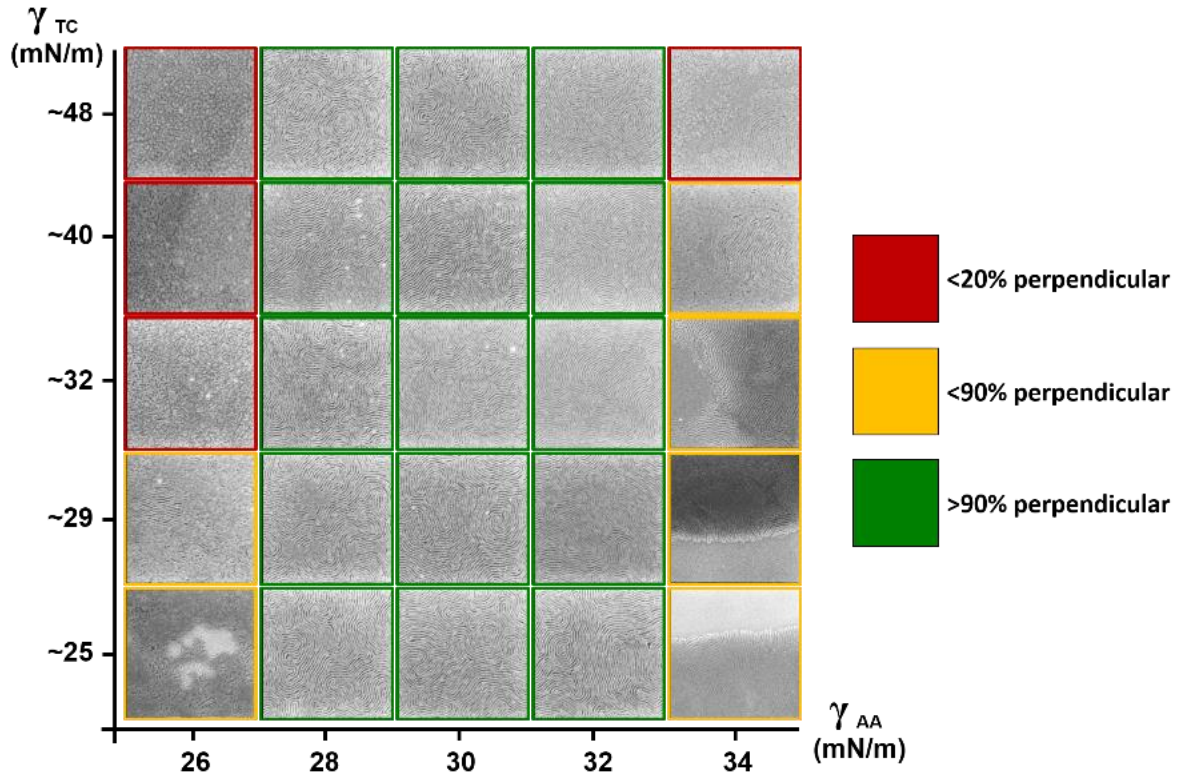

Figure 6. Cartography for the self-assembly of L-DBS18 coated on the AA materials as under-layers, as function of the surface energy of the various TCs. Cross-linking of the TCs by UV (180 mJ.cm^{-2}) followed by a 90°C-3 minutes bake. Thermal bake performed at 240°C-5mins. Magnification ×100000 with field area of 1.35 µm × 1.35 µm.

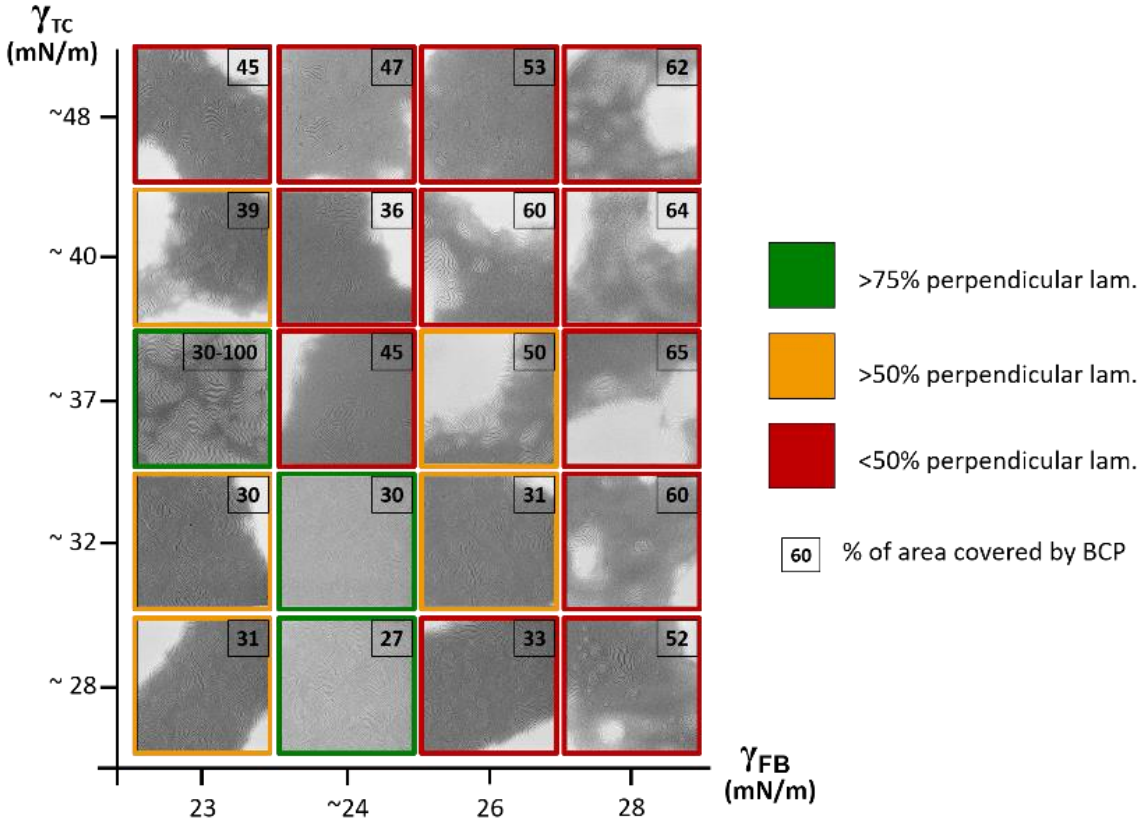

Figure 7. Cartography for the self-assembly of L-DBS18 coated on the FB materials as under-layers, as function of the surface energy of the various TCs. Cross-linking of the TCs by UV (180 mJ.cm^{-2}) followed by a 90°C-3 minutes bake. Thermal bake performed at 170°C-5mins to limit the dewetting of the BCP. Magnification ×100000 with field area of 1.35 µm × 1.35 µm.

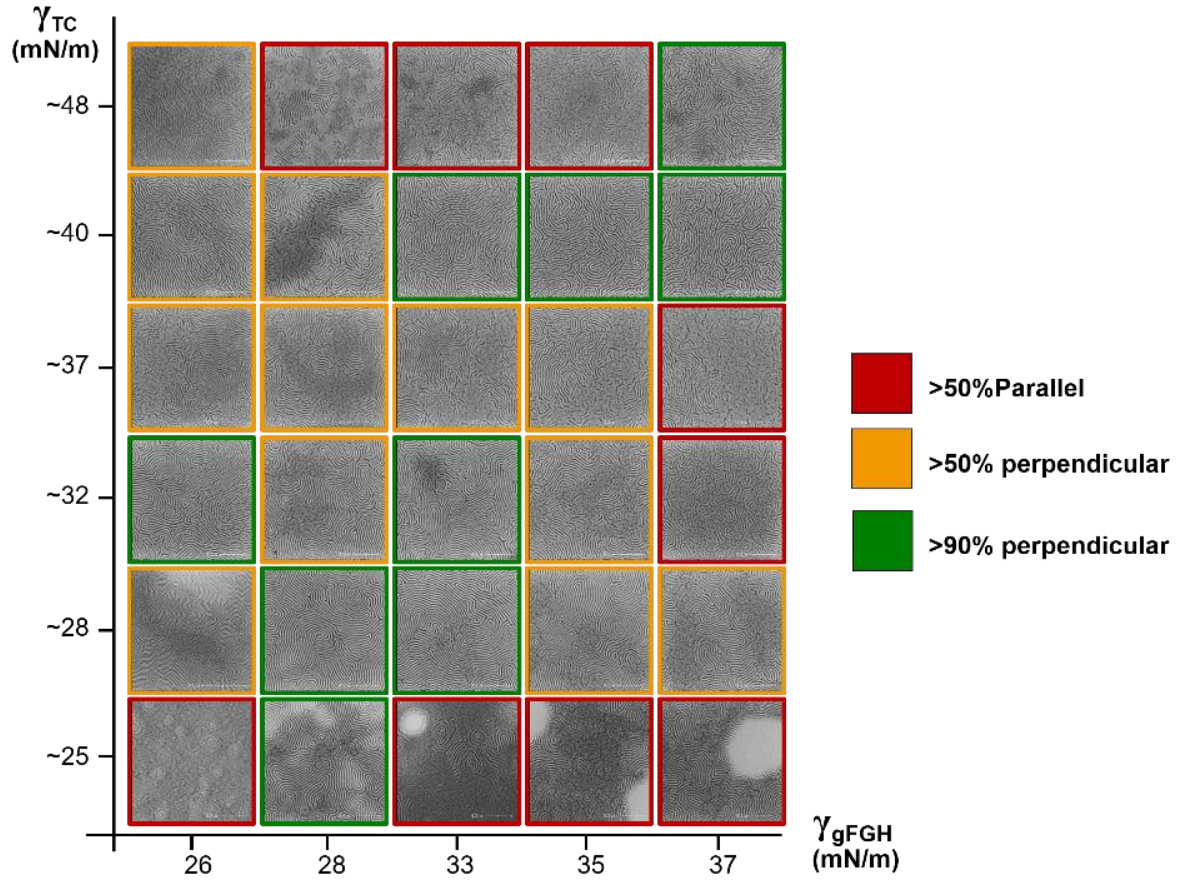

Figure 8. Cartography for the self-assembly of L-DBS18 coated on the grafted FGH materials (gFGH) as under-layers, as function of the surface energy of the various TCs. Cross-linking of the TCs by UV (180 mJ.cm^{-2}) followed by a 90°C-3 minutes bake. Thermal bake performed at 260°C-5mins. Magnification ×100000 with field area of 1.35 µm × 1.35 µm.

Interestingly, large differences in terms of lamellae orientation are observed by changing the substrate treatment. For the AA series, the UL composition largely influences the resulting lamellar orientation. Indeed, non-dewetted perpendicular lamellae are observed for three different ULs for all tested TCs (three central columns of the cartography shown in Figure 6). Outside of these conditions, dewetting and/or large areas with parallel lamellae are observed. Consequently, the contribution of the AA ULs to the BCP orientation seems to extend over the film thickness, independently of the TC.

For the FB series ULs (Figure 7), the thermal annealing to promote the BCP self-organization has to be limited to 170 °C to reduce the observed dewetting. Nevertheless, only few UL/TC combinations present areas with the desired perpendicular lamellar orientation. Comparison of the AA and FB ULs series highlights the fact that, the ULs surface energy is not sufficient to predict the BCP domain orientation. A more relevant parameter is the difference of interfacial energy of each block with the UL. Indeed, as reported in Table 2, an average value of this parameter is around 6 mN/m for the FB series while it is under 3 mN/m for the AA series (a perfect neutral layer is expected to present no interfacial energy differences). Accordingly, extended perpendicular orientations of the lamellae are retrieved with the AA series rather than the FB series. It should be noted that the lower $\Delta\gamma_i$ observed in a UL series does not correspond to the higher extent of perpendicular lamellae. These discrepancies might be due to several factors: the inaccuracy of the surface energy measurements (drop shape analysis error, despite statistical measurements performed over repeated samples for a given condition), the models used to compute the difference of interfacial tension, and the fact that the surface energies were measured at room temperature and not at the BCP annealing temperature.

Besides, the annealing temperature being different for both sets of experiments, the neutrality conditions and the self-organization kinetics are probably not exactly comparable.
The cartography obtained for grafted FGH layers onto the substrate is reported in Figure 8. Compared to the first AA series, the annealing temperature is almost the same (260 °C compared to 240 °C) while the scanned surface energy range and interfacial energy differences ($\Delta\gamma_i$) of the ULs with the BCP blocks are similar. Yet, the orientations of the lamellar structures are different. Here, the neutral window is restricted to intermediate surface energy values of ULs and TCs. Overall, it is more difficult to retrieve the desired perpendicular orientation of the lamellae on the gFGH series, despite predicted similar thermodynamic equilibrium conditions. We believe that these differences are due to a less efficient screening of the substrate in the case of gFGH, as regards to the AA series, according to their very low molecular masses, exacerbated by the high temperature processing for the self-assembly, leading to a potentially less-efficient "neutralization" of the interface. Also, these differences may be related to different self-assembly kinetics on the various UL chemistries.

CONCLUSIONS

In this work, we investigated the dewetting of thin layers of a lamellar-forming high-χ BCP in realistic nano-manufacturing conditions, i.e. the BCP layer is sandwiched between a brush grafted onto a silicon substrate and a chemically crosslinked top-coat. We demonstrated that both spinodal and nucleation-growth mechanism can be observed for the dewetting of these layers but that the self-organization kinetics appears to be faster than the dewetting process. Furthermore, while a BCP layer is shown to be thermodynamically unstable for neutral wetting conditions, a rigid TC is able to slow down dewetting leading to the formation of perpendicular nano-features. Finally, when comparing the neutrality performance of different UL chemistries, we observed different results that we tentatively ascribed to both the physico-chemical differences between the ULs and the interplay between the phase separation and dewetting kinetics processes. Our results demonstrated that additional studies are required for a full understanding of the interplay between self-assembly and dewetting in self-assembled BCP films.

ACKNOLEDGEMENTS

This work was supported by the REX-7 project from Région Rhône Alpes and BPI France, by the French RENATECH network, by the ANR LabEx Minos n°ANR-10-LABX-55-01 and by the ANR project BONSAI n°ANR-21-CE09-0009.

REFERENCES

[1] Park M 1997 Block Copolymer Lithography: Periodic Arrays of 10^11 Holes in 1 Square Centimeter *Science* **276** 1401–4

[2] Kim H-C C, Park S-M M, Hinsberg W D and Division I R 2010 Block copolymer based nanostructures: Materials, processes, and applications to electronics *Chemical Reviews* **110** 146–77

[3] Sinturel C, Bates F S and Hillmyer M A 2015 High X-Low N Block Polymers: How Far Can We Go? *ACS Macro Letters* **4** 1044–50

[4] Geoghegan M and Krausch G 2003 Wetting at polymer surfaces and interfaces *Progress in Polymer Science* **28** 261–302

[5] Gentili D, Foschi G, Valle F, Cavallini M and Biscarini F 2012 Applications of Dewetting in Micro and Nanotechnology *Chem. Soc. Rev* **41** 4430

[6] Brochard-Wyart F, de Gennes P G, Hervert H and Redon C 1994 Wetting and Slippage of Polymer Melts on Semi-ideal Surfaces *Langmuir* **10** 1566–72

[7] Brassat K and Lindner J K N 2020 Nanoscale Block Copolymer Self-Assembly and Microscale Polymer Film Dewetting: Progress in Understanding the Role of Interfacial Energies in the Formation of Hierarchical Nanostructures *Advanced Materials Interfaces* **7** 1901565

[8] Cheng G and Perahia D 2016 Dewetting and microphase separation in symmetric polystyrene-block-polyisoprene diblock copolymer ultrathin films *Polymer International* **65** 39–47

[9] Yan D, Huang H, He T and Zhang F 2011 Coupling of Microphase Separation and Dewetting in Weakly Segregated Diblock Co-polymer Ultrathin Films *Langmuir* **27** 11973–80

[10] Limary R and Green P F 1999 Dewetting Instabilities in Thin Block Copolymer Films: Nucleation and Growth *Langmuir* **15** 5617–22

[11] Müller-Buschbaum P, Gutmann J S, Lorenz-Haas C, Wunnicke O, Stamm M and Petry W 2002 Dewetting of Thin Diblock Copolymer Films: Spinodal Dewetting Kinetics *Macromolecules* **35** 2017–23

[12] Hamley I W, Hiscutt E L, Yang Y-W and Booth C 1999 Dewetting of Thin Block Copolymer Films *Journal of Colloid and Interface Science* **209** 255–60

[13] Legrain A, Fleury G, Mumtaz M, Navarro C, Arias-Zapata J, Chevalier X, Cayrefourcq I and Zelsmann M 2017 Straightforward Integration Flow of a Silicon-Containing Block Copolymer for Line-Space Patterning *ACS Applied Materials and Interfaces* **9** 43043–50

[14] Chevalier X, Gomes Correia C, Pound-Lana G, Bézard P, Sérégé M, Petit-Etienne C, Gay G, Cunge G, Cabannes-Boué B, Nicolet C, Navarro C, Cayrefourcq I, Müller M, Hadziioannou G, Iliopoulos I, Fleury G and Zelsmann M 2021 Lithographically Defined Cross-Linkable Top Coats for Nanomanufacturing with High-χ Block Copolymers *ACS Appl. Mater. Interfaces* **13** 11224–36

[15] Owens D and Wendt R 1969 Estimation of the Surface Free Energy of Polymers *J. Appl. Polym. Sci* **13** 1741–7

[16] Wu S 1971 Calculation of Interfacial Tensions in Polymer Systems *J. Polym. Sci* 43 19-30

[17] Matsen M W and Gardiner J M 2001 Autophobic dewetting of homopolymer on a brush and entropic attraction between opposing brushes in a homopolymer matrix *The Journal of Chemical Physics* **115** 2794–804

[18] Lee H, Lee W, Soo Han Y, Kim E and Ryu D Y 2016 Autophobic dewetting of polystyrenes on the substrates grafted with chemically identical polymers *Polym. J* **48** 503–7

[19] Mansky P, Lui Y, Huang E, Russell T P and Hawker C J 1997 Controlling Polymer-Surface Interactions with Random Copolymer Brushes *Science* **275** 1458–60

[20] Farrell R A, Kehagias N, Shaw M T, Reboud V, Zelsmann M, Holmes J D, Sotomayor Torres C M and Morris M A 2011 Surface-directed dewetting of a block copolymer for fabricating highly uniform nanostructured microdroplets and concentric nanorings *ACS Nano* **5** 1073–85

[21] Ferrarese Lupi F, Giammaria T J, Miti A, Zuccheri G, Carignano S, Sparnacci K, Seguini G, De Leo N, Boarino L, Perego M and Laus M 2018 Hierarchical Order in Dewetted Block Copolymer Thin Films on Chemically Patterned Surfaces *ACS Nano* **12** 7076–85

[22] Epps T H, DeLongchamp D M, Fasolka M J, Fischer D A and Jablonski E L 2007 Substrate Surface Energy Dependent Morphology and Dewetting in an ABC Triblock Copolymer Film *Langmuir* **23** 3355–62

[23] Russell T P, Menelle A, Anastasiadis S H, Satija S K and Majkrzak C F 1991 Unconventional morphologies of symmetric, diblock copolymers due to film thickness constraints *Macromolecules* **24** 6263–9

[24] Kikuchi M and Binder K 1994 Microphase separation in thin films of the symmetric diblock-copolymer melt *The Journal of Chemical Physics* **101** 3367–77